Thin Solid Films 560 (2014) 59–64

Contents lists available at ScienceDirect

Thin Solid Films

journal homepage: www.elsevier.com/locate/tsf

Understand the importance of molecular organization at polymer–polymer interfaces in excitonic solar cells

Helena M.G. Correia, Hélder M.C. Barbosa, Luís Marques, Marta M.D. Ramos *

Centre of Physics and Department of Physics, University of Minho, Campus de Gualtar, 4710-057 Braga, Portugal

ARTICLE INFO

Available online 25 October 2013

Keywords:
Monte Carlo modelling
Polymer–polymer interfaces
All polymer solar cells
Exciton dissociation
Charge transport

ABSTRACT

To improve the photovoltaic power conversion efficiency of organic solar cells it is necessary to increase the open circuit voltage and short circuit current. Prior work has shown that both these device properties can be improved by using donor–acceptor systems composed of two polymers, which favors excitons dissociation and charge generation, and subsequent charge transport to the electrodes. However, device performance depends strongly on the experimental conditions under which the device was created, because they determine the molecular structure of the interface between the two polymers. Polymer chains can have different conformations relative to the interface, creating different arrangements of the conjugated segments whose disorder degree can affect energy and charge transfer. Thus, understanding this effect is of utmost importance to improve the efficiency of all-polymer excitonic solar cells. In this work, we present the results obtained using a Monte Carlo model that takes into account the arrangement of the polymer strands at polymer–polymer interfaces and considers the main physical processes mediating exciton and charge dynamics. Our results show that the amount of charge extracted from the interface is sensitive to the orientation of polymer strands at interfaces and on the diffusive layer width formed by the mixture of both polymers.

1. Introduction

Organic solar cells (OSC) have received much attention in the last decade because of their low cost, low weight and easy fabrication, among other advantages, which enable large-scale fabrication and the production of flexible devices. A promising type of organic solar cell, the so-called all-polymer solar cells (all-PSC), consists of a mixture of two different semiconducting polymers, which works as donor–acceptor system favoring exciton dissociation/charge generation and charge transport to the respective electrodes. This type of solar cells presents potential advantages over other cells, such as polymer–fullerene OSC, because they can in principle reach higher open-circuit voltages, cover complementary regions of the solar spectrum, since both polymers can have complementary absorption spectra, and reach high efficiencies through appropriate control of nanomorphology by using block-copolymers or suitable deposition conditions [1–3]. However, the best efficiency reported so far for this type of organic solar cells is of 2% [4], much lower than the 10% maximum efficiency reported for polymer–fullerene systems and the reason for this low efficiency is not entirely clear [5].

One of the reasons proposed for the low-efficiency of all-PSC is the presence of a layer composed of a mixture of donor and acceptor polymers at the interface between the two pristine polymer domains that make up the all-PSC [6]. This interfacial layer is unstructured, and thus typically called a diffusive layer, and has nanoscale dimensions. Although it would be expected that an increase in the diffusive layer width could improve the efficiency of all-PSC, previous experimental and theoretical studies have shown that wider diffusive layers increase exciton quenching at the interface but do not increase current density [7]. This loss of device performance was ultimately attributed not directly to the increase in width of the diffusive layer, but to the simultaneous increase in thickness of the two pristine polymer domains on either side of the diffusive layer. Following studies performed by Marsh et al. [8], larger polymer domains were shown to influence the processes subsequent to exciton dissociation: larger domains reduce the number of connections between them and thus decrease the number of pathways for charge transport towards the electrodes. As a result of charge accumulation, there is an increase of coulomb interaction between the geminate charge pairs, which favors charge recombination, consequently the amount of collected charge and thus the device efficiency are reduced. Mori et al. [4] reported recently that it is possible to control the width of the diffusive layer by the proper choice of the deposition conditions and post deposition treatment. However, the same study shows that this experimental control of the diffusive layer thickness also leads to a change in the size of polymer domains. These results suggest that it may be possible to optimize the relative sizes of the diffusive layer and the pristine polymer domains to maximize exciton dissociation, charge moving away from the diffusive layer and charge percolation along the polymer domains. Doing so requires that the dependence of the optoelectronic processes with the size of each domain and the width of the diffusive layer at the polymer–polymer

* Corresponding author. Tel.: +351 253 604 330; fax: +351 253 678 981.
E-mail address: marta@fisica.uminho.pt (M.M.D. Ramos).

0040-6090/$ – see front matter © 2013 Elsevier B.V. All rights reserved.
http://dx.doi.org/10.1016/j.tsf.2013.10.057

interface is understood. With this in mind, recent studies have investigated the influence of the diffusive layer thickness in all-PSC with polymer bilayer architecture. According to Yan et al. [9], annealing the active layer increases the width of the diffusive layer and simultaneously reduces charge mobility in the pure domains. These observations were explained by an increased charge confinement within the diffusive layer. Although Yan's results establish a relationship between the loss of efficiency in all-PSC and the combined effect of the diffusive layer width, polymer domain size and different charge mobility on both polymer materials, they do not give a clear picture about the loss mechanisms occurring in the diffusive layer nor do they clarify the effect of each individual material characteristic on all-PSC efficiency. Furthermore, the effect of polymer orientation/conformation details at molecular scale on exciton dissociation/charge separation was not considered in any of the studies mentioned above, even though polymer orientation/conformation can have an important role in all-PSC efficiency [10]. There is thus a clear need for a computational modelling approach which includes the molecular arrangement at the polymer–polymer interface to assess the influence of the thickness of the diffusive layer on charge generation.

To clarify this issue, we developed a dynamic Monte Carlo (MC) model that is quite different from the ones already published, since it considers explicitly the arrangement of the conjugated polymer segments. The model uses results from quantum molecular dynamics calculations as input parameters for the Monte Carlo simulations. In this work we consider the molecular properties of poly[p-phenylene vinylene] (PPV) and poly[7-cyano-p-phenylene vinylene] (7-CN-PPV), since they are well known polymers and their derivatives are used in all-PSC to form donor–acceptor interfaces [2].

2. Theoretical methods and computational details

Unravelling the effect of the presence of a diffusive layer on the optoelectronic processes governing charge generation at that polymer–polymer interface can easily be achieved by computational modelling at the microscopic scale. This approach makes it possible to include the characteristic details of molecular arrangement at nanoscale that can influence the physical processes mediating the dynamics of excitons (i.e. diffusion and dissociation) and charges (i.e. transport and recombination).

It is possible to find in the literature several microscopic models to study organic solar cells, which consider the main physical processes that underlie the functioning of this type of device, and, at some point, the influence of the nanomorphology on its performance. Most of these models study the effect of interfaces in the optoeletronic processes of organic solar cells made of a polymer–fullerene blend, as the ones proposed by Heiber et al. [11] and Eersel et al. [12]. However, the results of these studies yield little insight into charge generation at polymer–polymer interfaces because the properties of fullerenes are quite different from polymers. Walker et al. [13] and Marsh et al. [8] presented microscopic models to study the influence of the interface area between two polymers on the internal quantum efficiency and in the efficiency of geminate charge separation of OSC. Although the results obtained by both models explain the experimental results for solar cells made of polymer blends, they only focus on the effect of bulk heterojunction interface area on the device functioning and do not consider the effect of the presence of a diffusive layer of both materials at the interface. Recently more realistic microscopic models to understand the role of the intermixing zone present at the polymer–polymer interface were proposed [9,14]. However, these models assume that the donor–acceptor sites can be seen as a Cartesian distribution of points, i.e., they neglect the effect of the orientation of the interfacial polymer strands on the optoelectronic processes that occur at these interfaces. Previous works have shown that exciton dynamics is affected by the spatial orientation of the polymer strands [15] and the efficiency of charge separation depends on the polymer chain conformation at molecular scale [10]. On the other hand, several results show that the anisotropic charge transport observed in polymeric films is associated with the relative orientation of the polymer strands [16]. More importantly, the models proposed by Yan et al. [9] and Lyon et al. [14] assigned to each site an energy taken from a Gaussian-distribution to simulate the effects of the energetic disorder for exciton and charge transport. The mean value and width (σ) of this distribution was chosen to best fit the electronic properties of the polymers considered. This strategy thus does not establish a clear link between the energetic disorder, that mediates charge and exciton transport, to the polymer chemical structure and to the varying conjugated segment length characteristic of the semiconducting polymers. The model proposed by us here, explicitly makes this link, since it includes a detailed description of the spatial arrangement of the polymer conjugated segments at the donor–acceptor interface and the influence of segment length on the molecular properties, which affect the energetic disorder for exciton and charge dynamics. Our model thus allows a deeper investigation of the effect of the diffusive layer thickness at the polymer–polymer interface on the exciton dissociation, charge recombination and charge generation than existing ones.

2.1. Spatial molecular arrangement.

The challenge of controlling polymer–polymer interfaces depends on device architecture (bilayer or blend). For a bilayer architecture, sharp interfaces [17] and diffusive interfaces with different diffusive layer thicknesses [9] can easily be achieved. In order to separate the simultaneous effects of changing the thickness of the diffusive layer and the size of both donor and acceptor polymer nanodomains on device performance observed in the experiments, we consider in this work a bilayer polymer solar cell architecture with a fixed thickness between the electrodes, the same thickness for both donor (PPV) and acceptor (7-CN-PPV) pristine polymers and a diffusive layer with varying thickness at the middle of the device with a composition 1:1 in terms of monomers of both polymers.

The usual way to model a conjugate polymer chain is by considering it an array of conjugated segments with varying number of monomers, connected by kinks and twists along the polymer backbone [18]. Therefore, the nanomorphology of each polymer within the pristine layer is reduced to the spatial arrangement of the conjugated segments of that material, and the diffusive layer formed at polymer–polymer interface can be seen as an array of equal number of conjugated segments of both polymers with uniform distribution.

To build our polymer networks we proceed as follows:

i) each conjugated segment behaves as a straight rigid rod, the minimal distance between two rods (i.e. minimum intermolecular distance) (Fig. 1a) is 0.650 nm, based on self-consistent quantum molecular dynamics calculations [19];
ii) each rod is randomly placed in a box with 100 nm (model axis) per 20×20 nm, the length of each rod is taken from a Gaussian distribution of lengths with a mean value of 7 monomers (Fig. 1b), the typical average conjugation length predicted for the semiconducting polymers considered in this work [20];
iii) conjugated segments are placed inside the box with the molecular axis parallel to the electrodes surface and random orientation in the plane parallel to the electrodes surface, which mimics well the spatial orientation of those segments obtained by the spin-coating deposition technique used in the experiments. The different distances and orientations between the molecular axes of the polymer strands reflect the spatial disorder that characterizes polymer morphology at the nanoscale. This approach has been validated by the simulation work of charge and exciton transport in conjugated polymers by Athanasopoulos et al. [21,22], with a similar nanomorphology.
iv) In our work we consider two types of interfaces present in our bilayer networks: sharp and diffusive. The sharp interface is realized

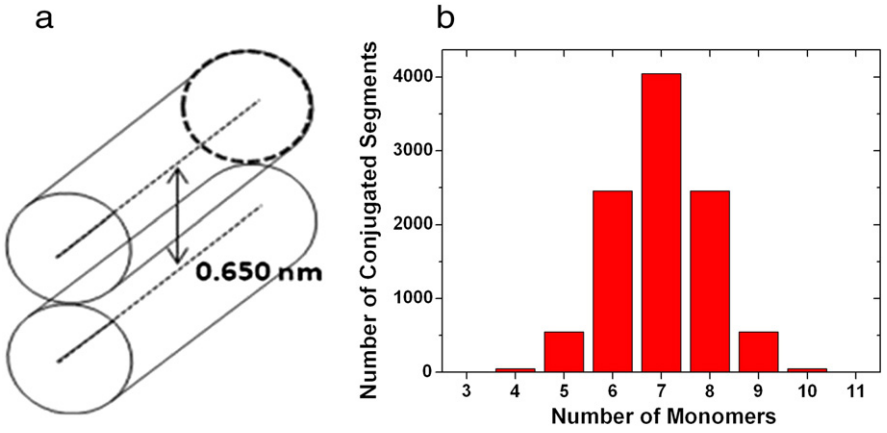

Fig. 1. (a) Minimum intermolecular distance allowed between polymer strands in the polymer networks. (b) Number of conjugated segments with a specific length measured in monomers units present in the polymer networks.

by placing strands of the acceptor polymer in the region that goes from 0 nm to 50 nm, and strands of the donor polymer in the region that goes from 50 nm to 100 nm (Fig. 2a). When the upper/lower limit of the acceptor (7-CN-PPV)/donor (PPV) polymer increases/decreases by the same amount, a mixture of both polymer strands is realized in the central region of the device creating a diffusive layer between the pristine donor and acceptor layers. By controlling these limits it is possible to have polymer networks with a diffusive layer with well-defined widths (Fig. 2b).

For each type of interface we used 10 different polymer network realizations. All polymer networks had the same density to within 1%, to guarantee that the results are not influenced by significant variations of this parameter. For each network realization, 30 MC simulations were performed.

2.2. Rules for the optoelectronic processes

2.2.1. Rules for exciton dynamics

Exciton dynamics in polymeric films is mainly mediated by the processes of diffusion and quenching at the polymer–polymer interface. In our simulations, we impose an exciton creation rate to allow low exciton densities in order to neglect any exciton–exciton interaction mechanisms [23]. We consider only the formation of Frenkel-type singlet excitons, since atomistic calculations showed that singlet excitons are created in the central region of conjugated segments, leading to a dipole-type charge distribution [24]. Each exciton has an intrinsic lifetime given by:

$$t_i = -\frac{\ln(X)}{w_{0,\mathrm{Exciton}}} \tag{1}$$

with X a random number between 0 and 1, and $w_{0,\mathrm{Exciton}}$ the decay probability of the excited state per unit time by spontaneous photon emission (radiative decay rate).

In our model, we assume that the exciton diffusion mechanism is mediated by dipole–dipole interaction, where exciton percolation is thermally activated and occurs by hopping between the central regions of the neighboring conjugated segments. The exciton hopping rate is given by:

$$w_{\mathrm{hop,Exciton}} = w_{0,\mathrm{dip-dip}} \times \begin{cases} 1 & for \quad r_{ij}<R \\ \left(\frac{R}{r_{ij}}\right)^6 & for \quad r_{ij}\geq R \end{cases} \times \begin{cases} 1 & \text{for} \quad \Delta E_{ij}<0 \\ \exp\left(-\frac{\Delta E_{ij}}{kT}\right) & \text{for} \quad \Delta E_{ij}\geq 0 \end{cases} \tag{2}$$

In this expression $w_{0,\mathrm{dip-dip}}$ is the maximum exciton hopping frequency between conjugated polymer segments, R is the critical distance above which the hopping frequency depends on the distance between the central region of the polymer strands (r_{ij}), ΔE_{ij} is the energy barrier that an exciton has to overcome for hopping between strands, k is the Boltzmann constant and T is the temperature. Since we assume

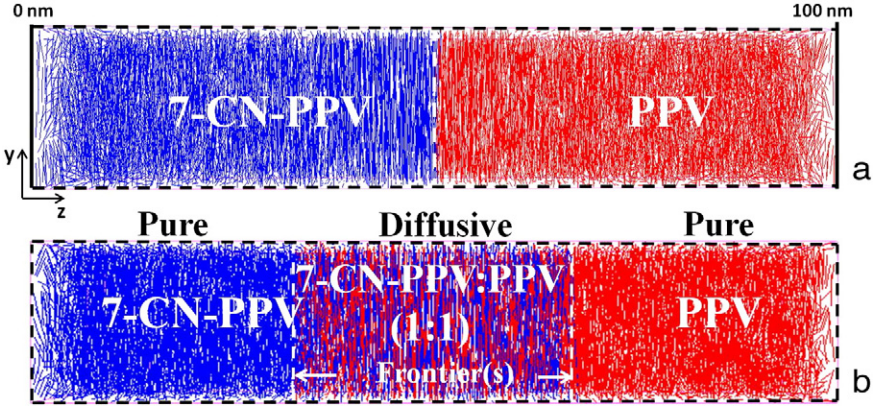

Fig. 2. Polymer–polymer layers with (a) a sharp interface, (b) a diffusive interface seen as a heterojunction composed by a 1:1 mixture of both polymers (i.e. diffusive layer) limited by pure polymer layers.

a dipole–dipole interaction mechanism for exciton hopping, R is given by:

$$R^6 = R_0^6 \times \left[\cos\left(\theta_{ij}\right) - 3\cos(\theta_i)\cos\left(\theta_j\right)\right]^2 \quad (3)$$

where R_0 is the electron–hole distance (i.e. dipole length) in a singlet exciton formed in a polymer strand, extracted from atomistic calculations [24], θ_{ij} is the angle between the dipole directions in strands i and j involved in the hopping process and $\theta_{i(j)}$ is the angle between the dipole direction of strand $i(j)$ and the hopping direction.

When an exciton localized on a PPV strand reaches a polymer strand of 7-CN-PPV that works like electron acceptor, it easily dissociates into a pair of charges, due to the polymers' molecular properties [25]. Since we assume that an exciton behaves like a bounded electron–hole pair, in our model the dissociation process occurs by electron hopping from the donor polymer (PPV strand) to the acceptor polymer (7-CN-PPV strand), the dissociation rate being given by:

$$w_{\text{Diss.,Exciton}} = w_{0,\text{Diss.}} \times \begin{cases} 1 & \text{for} \quad r_{ij} < r_0 \\ \exp\left(-\dfrac{r_{ij}-r_0}{r_0}\right) & \text{for} \quad r_{ij} \geq r_0 \end{cases} \times \begin{cases} 1 & \text{for} \quad \Delta E_{ij} < 0 \\ 0 & \text{for} \quad \Delta E_{ij} \geq 0 \end{cases} \quad (4)$$

where $w_{0,\text{Diss.}}$ is the maximum exciton dissociation frequency, r_{ij} is the hopping distance and r_0 is the minimal distance between nearest polymer strands. ΔE_{ij} is the energy barrier that the electron has to overcome in order for exciton dissociation to occur. This energy barrier is given by:

$$\Delta E_{ij} = \text{IP}_\text{D} - \text{EA}_\text{A} - E_{\text{Exc.}} - \Delta U + E_{\text{GP}} \quad (5)$$

being E_{Exc} the singlet exciton energy, IP is the ionization potential of the donor, EA is the electron affinity of the acceptor, ΔU is the electric bias between donor and acceptor positions that results from the local electric field, and E_{GP} is the binding energy of the geminate pair due to electron–hole electrostatic attraction. The IP and EA values were obtained from atomistic calculations [26].

2.2.2. Rules for charge dynamics

After exciton dissociation into a pair of charges of opposite sign, charges can hop between polymer strands, due to the presence of a local electric field. During the simulations, a charge can be trapped inside the polymer network, recombine with a charge of opposite sign or reach the electrode to be collected. In our model we assume that charge transport occurs by a hopping process mediated by the local electric field. The charge hopping rate is given by:

$$w_{\text{Hop,Charge}} = w_{0,\text{Charge}} \times \cos\theta \times \begin{cases} 1 & \text{for} \quad r_{ij} < r_0 \\ \exp\left(-\dfrac{r_{ij}-r_0}{r_0}\right) & \text{for} \quad r_{ij} \geq r_0 \end{cases} \times \begin{cases} 1 & \text{for} \quad \Delta E_{ij} < 0 \\ \exp\left(-\dfrac{\Delta E_{ij}}{kT}\right) & \text{for} \quad \Delta E_{ij} \geq 0 \end{cases} \quad (5)$$

$w_{0,\text{Charge}}$ represents the maximum charge hopping frequency between nearest polymer strands. The second term ($\cos\theta$) represents the influence of the direction of the local electric field along the hopping distance (r_{ij}). The local electric field is the sum of the applied electric field, the field due to charge distribution within the polymer network, and the field due to electrode polarization. r_0 is the minimal distance between nearest polymer strands and ΔE_{ij} is the energy barrier height that a charge has to overcome to hop between polymer strands. The energy barrier height for an electron (hole) depends on the electron affinity (ionization potential) of the polymer strands and the bias voltage between the two sites that result from the local electric field.

During charge percolation inside the polymer network, a charge can recombine, if it meets a charge of opposite sign in the same strand, or be stored for a long time in energetic favorable strands. Table 1 summarizes the parameters assumed in our simulations.

Table 1
Parameters used in our simulations.

Parameter	Value
$w_{0,\text{Exciton}}$ (s^{-1})	1×10^9 [24]
$w_{0,\text{dip-dip}}$ (s^{-1})	3.3×10^{11} [25]
R_0 (nm)	1.30 [21]
$w_{0,\text{Diss.}}$ (s^{-1})	1×10^{12}
$w_{0,\text{Charge}}$ (s^{-1})	1×10^9 [26]
r_0 (nm)	0.650 [18]
T (K)	300

For each exciton or charge present in the polymer network, the only process that takes place is the one with the greatest hopping rate (w_{ij}), being the time of the event execution given by:

$$\tau = -\frac{\ln(X)}{w_{ij}} \quad (6)$$

where X is a random number uniformly distributed between 0 and 1.

To follow time evolution in our simulations, we implemented a strategy based on the first reaction method (FRM) [27]. For each simulation, a queue of time events is established for excitons, on the first computer interaction, or for excitons and charges, in the subsequent interactions, with increasing time. In each interaction, the event with the smallest execution time takes place, this time being subtracted from the remaining time of execution of the other events. This event is then removed from the queue and other events can be introduced. In our simulations a minimum of 3×10^4 trajectories associated to excitons formation was imposed, to guarantee that a steady state is achieved with no significant changes on the parameters measured.

3. Results and discussion

By using our Monte Carlo model, we perform computational experiments using the polymer networks with the interfaces described previously (see Fig. 2), with a constant exciton formation rate and an external applied electric field of 1.0 MV/cm. The model allows the calculation, among other parameters, of the yield on exciton dissociation, recombination events and charge extraction, which is the charge reaching the electrodes contributing to photoelectric effect, assuming as a reference the amount of excitons created until the steady state is reached. Fig. 3 shows the influence of sharp and diffusive polymer–polymer interface on the main optoelectronic processes that excitons and charges are involved in. Our results show that the presence of a diffusive interface leads to an increase on exciton quenching when compared to the sharp interface (i.e. 0 nm diffusive layer width). Moreover, the increase of the diffusive layer thickness also leads to an increase on exciton quenching. The presence of the diffusive layer at the polymer–polymer interface leads to an interpenetration of strands of both polymers, creating a mesh of donor–acceptor sites where excitons can easily dissociate. The probability of an exciton dissociation event occurring instead of exciton decay increases with the diffusive layer width, which agrees well with previous works [7]. However, the increase of exciton dissociation with the diffusive layer width is accompanied by an increase of charge recombination, and the difference between these two processes leads to a small yield of charge generation at the polymer–polymer interface that can contribute to the current density (i.e. charge extraction) (see Fig. 3).

Our results show a very interesting feature. For the molecular organization similar to the one obtained using the spin-coating technique, the charge extraction from the polymer–polymer interface, which contributes to the device efficiency, increases with the increase of the diffusive layer thickness until a certain value (8 nm for the 7-CN-PPV:PPV system) and decreases for thicknesses greater than that value,

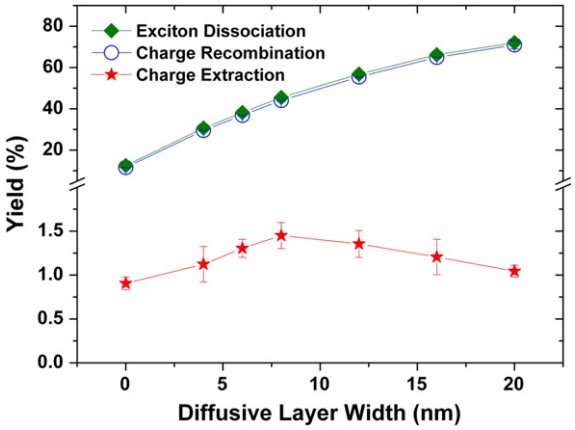

Fig. 3. Yield on exciton dissociation (diamonds), charge recombination (open circles), and charge extraction (stars) from polymer–polymer diffusive interfaces with different widths. The error bars show the maximum absolute deviation.

in agreement with the experimental works of MacNeill et al. [7] and Yan et al. [9]. The optimal thickness of the diffusive layer to maximize the charge extraction should be different for different polymeric systems because it depends on the molecular properties of the polymeric system. Since we assume pristine polymer domains with the same size and select donor and acceptor polymers with similar mobility for electrons and holes, we can conclude that the existence of an optimal thickness for the diffusive layer is an intrinsic effect of the interface formation and it is not a result of the change in polymer domain size and charge mobility suggested by the experiments.

To understand the factors that contribute to the behavior of charge separation shown in Fig. 3 we present in Table 2 the distribution of exciton formation, exciton decay, exciton dissociation and charge recombination within the pristine polymer layer, the diffusive layer and the interfaces between pristine and diffusive layers.

The results show the following features. First, for all diffusive layer thicknesses, the large majority of the excitons created within the diffusive layer and within the pristine/diffusive interface dissociate, with the exciton decay being negligible. Second, in these regions the exciton dissociation is larger than the difference between exciton formation and exciton decay, which suggests that part of the excitons dissociated in those regions are created on the neighbor regions, diffusing efficiently to the diffusive layer and dissociating at the pristine/diffusive layer interfaces. Third, almost all charges created due to exciton dissociation within the diffusive layer recombine. Fourth, although charge recombination is lower than exciton dissociation at pristine/diffusive layers interfaces, the charge generation at the interface is much higher than the charge collected at the electrodes due to the large amount of recombination taking place within the pristine layers near those interfaces. Our results are in good agreement with experiments but disagree with those obtained using simulations by Lyons et al. [14] because they consider the polymer morphology as a Cartesian distribution of points, an assumption that does not describe properly the effect of spatial and orientation disorder of polymer strands on charge recombination.

There is experimental evidence that some post treatments can lead to a change in molecular conformation. To assess this effect we have performed the same calculations with a random orientation (not shown) of the conjugated polymer segments throughout the device, thus mimicking an amorphous structure. For this molecular orientation we found lower charge generation at the polymer–polymer interface, which does not change with the thickness of the diffusive layer. This result shows that we need to be cautious when analyzing the experimental results, because a decrease in charge generation at the polymer–polymer interface could not be associated with an increase in the thickness of the diffusive layer as a result of the post-treatment, but only to a change in the molecular arrangement at the interface.

The need for controlling morphology on polymer blends on such small length scales, as our results show, can be a challenging task, but exploring the use of non-conventional methods like chemical additives [28], application of external voltages [29] or using co-polymers [30], can lead to a control of the molecular arrangement at polymer–polymer interfaces with promising results as the ones shown here.

4. Conclusions

We have presented a study to unravel the role of the diffusive layer present at polymer–polymer interfaces on the functioning of all-polymer solar cells to understand under which conditions the diffusive layer can maximize charge generation and thus improve device efficiency. Our results clearly show that the diffusive layer can act as a loss of efficiency channel, by confining charge and promoting geminate charge recombination, even in the absence of other factors that can contribute to this confinement. However, by manipulating the molecular organization at the polymer–polymer interface it is possible improve charge separation from the interface with the aim of increasing all-PSC efficiency.

Although there is much to improve in the functioning of all-polymer solar cells so that they can compete with the state-of-art polymer–fullerene solar cells, there are good perspectives for this type of solar cells to play an important place in the photovoltaic market.

Acknowledgments

This research is partially sponsored by FEDER funds through the program COMPETE — Programa Operacional Factores de Competitividade and by national funds through FCT-Fundação para a Ciência e a Tecnologia, under the projects CONC-REEQ/443/EEI/2005 and PEst-C-FIS/UI607/2011-2012. We also are indebted to FCT and POPH for financial support the post-doctoral grants no SFRH/BPD/64554/2009 (H.M.G.C.) and no SFRH/BPD/80561/2011 (H.M.C.B.).

Table 2
Rate of exciton formation (Exc.), exciton decay (Dec.), exciton dissociation (Diss.) and charge recombination (Rec.) occurring in different regions of the simulated polymer bilayer, for different thicknesses of the diffusive layer.

Diffusive layer thickness	Pristine layers				Diffusive layer				Pristine/diffusive interfaces			
	Exc.	Dec.	Diss.	Rec.	Exc.	Dec.	Diss.	Rec.	Exc.	Dec.	Diss.	Rec.
0	94.36	87.37	0.03	6.47	0.00	0.00	0.00	0.00	5.64	0.01	12.37	4.96
4	79.31	69.16	0.00	5.22	10.20	0.00	14.40	14.52	10.49	0.03	16.18	9.74
6	71.30	61.66	0.00	5.18	19.31	0.00	21.74	22.45	9.39	0.05	16.37	9.20
8	63.89	54.37	0.03	5.28	27.34	0.01	30.27	30.60	8.77	0.00	15.15	8.13
12	50.80	43.08	0.00	4.13	41.40	0.02	44.38	44.10	7.80	0.00	12.37	7.18
16	40.08	33.73	0.00	3.54	52.80	0.06	55.38	55.22	7.12	0.00	10.71	6.11
20	32.74	27.45	0.00	2.92	61.64	0.26	62.88	62.85	5.62	0.21	9.09	5.11

References

[1] C.R. McNeill, N.C. Greenham, Adv. Mater. 21/38–39 (2009) 3840.
[2] S.C. Veenstra, J. Loos, J.M. Kroon, Prog. Photovoltaics 15/8 (2007) 727.
[3] E.J. Zhou, J.Z. Cong, Q.S. Wei, K. Tajima, C.H. Yang, K. Hashimoto, Angew. Chem. Int. Ed. 50/12 (2011) 2799.
[4] D. Mori, H. Benten, J. Kosaka, H. Ohkita, S. Ito, K. Miyake, ACS Appl. Mater. Interfaces 3/8 (2011) 2924.
[5] C.R. McNeill, Energy Environ. Sci. 5 (2) (2012) 5653.
[6] S. Swaraj, C. Wang, H.P. Yan, B. Watts, L.N. Jan, C.R. McNeill, H. Ade, Nano Lett. 10/8 (2010) 2863.
[7] C.R. McNeill, S. Westenhoff, C. Groves, R.H. Friend, N.C. Greenham, J. Phys. Chem. C 111/51 (2007) 19153.
[8] R.A. Marsh, C. Groves, N.C. Greenham, J. Appl. Phys. 101/8 (2007).
[9] H.P. Yan, S. Swaraj, C. Wang, I. Hwang, N.C. Greenham, C. Groves, H. Ade, C.R. McNeill, Adv. Funct. Mater. 20/24 (2010) 4329.
[10] T.W. Holcombe, J.E. Norton, J. Rivnay, C.H. Woo, L. Goris, C. Piliego, G. Griffini, A. Sellinger, J.-L. Bredas, A. Salleo, J.M.J. Frechet, J. Am. Chem. Soc. 133/31 (2011) 12106.
[11] M.C. Heiber, A. Dhinojwala, J. Chem. Phys. 137/1 (2012).
[12] H. van Eersel, R.A.J. Janssen, M. Kemerink, Adv. Funct. Mater. 22/13 (2012) 2700.
[13] P.K. Watkins, A.B. Walker, G.L.B. Verschoor, Nano Lett. 5/9 (2005) 1814.
[14] B.P. Lyons, N. Clarke, C. Groves, Energy Environ. Sci. 5/6 (2012) 7657.
[15] H.M.C. Barbosa, H.M.G. Correia, M.M.D. Ramos, J. Nanosci. Nanotechnol. 10/2 (2010) 1148.
[16] B. O'Connor, R.J. Kline, B.R. Conrad, L.J. Richter, D. Gundlach, M.F. Toney, D.M. DeLongchamp, Adv. Funct. Mater. 21/19 (2011) 3697.
[17] A. Charas, H. Alves, L. Alcacer, J. Morgado, Appl. Phys. Lett. 89/14 (2006).
[18] H.M.G. Correia, H.M.C. Barbosa, L. Marques, M.M.D. Ramos, Comput. Mater. Sci. 75 (2013) 18.
[19] M.M.D. Ramos, A.M. Almeida, H.M.G. Correia, R.M. Ribeiro, A.M. Stoneham, Appl. Surf. Sci. 238/1–4 (2004) 438.
[20] B.G. Sumpter, P. Kumar, A. Mehta, M.D. Barnes, W.A. Shelton, R.J. Harrison, J. Phys. Chem. B 109/16 (2005) 7671.
[21] S. Athanasopoulos, E. Hennebicq, D. Beljonne, A.B. Walker, J. Phys. Chem. C 112/30 (2008) 11532.
[22] S. Athanasopoulos, J. Kirkpatrick, D. Martinez, J.M. Frost, C.M. Foden, A.B. Walker, J. Nelson, Nano Lett. 7/6 (2007) 1785.
[23] I.G. Scheblykin, A. Yartsev, T. Pullerits, V. Gulbinas, V. Sundstroem, J. Phys. Chem. B 111/23 (2007) 6303.
[24] M.M.D. Ramos, H.M.G. Correia, Appl. Surf. Sci. 248/1–4 (2005) 450.
[25] S.D. Baranovskii, M. Wiemer, A.V. Nenashev, F. Jansson, F. Gebhardt, J. Phys. Chem. Lett. 3/9 (2012) 1214.
[26] H.M.G. Correia, PhD Thesis, University of Minho, Braga, 2007.
[27] J.J. Lukkien, J.P.L. Segers, P.A.J. Hilbers, R.J. Gelten, A.P.J. Jansen, Phys. Rev. E. 58/2 (1998) 2598.
[28] A.J. Moule, K. Meerholz, Adv. Mater. 20/2 (2008) 240.
[29] S.Y. Ma, Y.M. Shen, P.C. Yang, C.S. Chen, C.F. Lin, Org. Electron. 13/2 (2012) 297.
[30] P.D. Topham, A.J. Parnell, R.C. Hiorns, J. Polym. Sci. Part B: Polym. Phys. 49/16 (2011) 1131.